# Effect of surface functionalization of Fe3O4 nano-enabled electrodes on the electrochemical reduction of nitrate

Mariana Marcos-Hernández, Gabriel Antonio Cerrón-Calle, Yulu Ge, Sergi Garcia-Segura, Carlos M Sánchez-Sánchez, Ana Sofia Fajardo, Dino Villagrán

# Effect of surface functionalization of $Fe_3O_4$ nano-enabled electrodes on the electrochemical reduction of nitrate

Mariana Marcos-Hernández[a,b], Gabriel Antonio Cerrón-Calle[a,c], Yulu Ge[a,b], , Sergi Garcia-Segura[a,c], Carlos M. Sánchez-Sánchez[d], Ana S. Fajardo[a,c,d,*], Dino Villagrán[a,b,**]

[a]*Nanosystems Engineering Research Center for Nanotechnology-Enabled Water Treatment*

[b]*Department of Chemistry and Biochemistry, The University of Texas at El Paso, El Paso, TX 79968, USA*

[c]*School of Sustainable Engineering and the Built Environment, Arizona State University, Tempe, Arizona 85287-3005, United States*

[d]*Sorbonne Université, CNRS, Laboratoire Interfaces et Systèmes Electrochimiques (LISE), 4 place Jussieu, F-75005, Paris, France*

**Corresponding author**

***Ana Sofia Fajardo, E-mail: adossan3@asu.edu

****Dino Villagran, E-mail: dino@utep.edu

**Abstract**

Nitrate is a noxious and persistent oxyanion in drinking waters. It is themed as one of the most common water quality violations worldwide. Nitrate electrocatalytic reduction appears to be a viable solution. However, the use of platinum group elements (PGEs) as electrocatalysts must be avoided due to their high cost and limited availability. In this study, earth-abundant nano-$Fe_3O_4$ electrodes were synthesized to surpass those implementation barriers. Surface functionalization has demonstrated to impact performance of inner sphere catalytic transformations but has been seldomly explored in the context of nitrate remediation. To understand the effect of the functionalization of $Fe_3O_4$ surfaces, $Fe_3O_4$ nano-enabled electrodes were functionalized with amine and carboxylic acids groups. After 360 min, the most promising results were obtained when the $Fe_3O_4$ surface was modified with carboxylic groups. The nitrate conversion obtained was ~90%, selectivity towards ammonia of ~55% and an electric energy per order (EE/O) of 37 kWh $m^{-3}$ $order^{-1}$. This EE/O value is ~2x lower, when compared to an experiment using a bare Fe-plate. Therefore, nano-$Fe_3O_4$ electrodes hold the potential of providing a green resource recovery process to treat nitrate pollution while recovering ammonia for its reuse as enriched water for crops irrigation.

*Keywords*: nano-enabled electrodes; functionalized magnetite; water denitrification; nitrate electroremediation; mineral iron oxide

## 1. Introduction

Nitrate is one of the top ten drinking water contaminants worldwide causing major environmental and health concerns [1–5]. Exposure to levels higher than 10 mg $NO_3^-$-N $L^{-1}$ relate to a wide range of human ailments, such as: cancer, thyroid problems, and methemoglobinemia (blue baby syndrome) [2,6,7]. Nitrate concentration in natural waters has increased dramatically due to anthropogenic nitrogen-based fertilizer runoff from agricultural lands, animal manure, and sewage discharges [8,9]. In the United States, over 40 million people rely on private groundwater wells that may contain nitrate concentrations above regulated limits [10,11]. Easy to operate technologies that can locally treat nitrate polluted water sources is a need to enhance water quality for all [12].

Conventional nitrate removal technologies are based on ion exchange and biological processes [13,14]. However, these technologies generate brines or sludge and cannot be easily deployed as decentralized treatment systems [15,16]. Electrochemical reduction of nitrate (ERN) emerges as a promising technology for water denitrification. Product selectivity is necessary for the implementation of ERN technologies as fit-for-purpose applications. Nitrate can be reduced to nitrogen gas ($N_2$) or ammonia ($NH_3$) as suitable final products in water treatment applications. Nitrogen gas is inert and it is the preferred product for drinking water treatment [17,18]. However, there is an increasing interest for the product selectivity towards ammonia as a valuable commodity chemical [19,20]. Besides reducing the environmental burden of nitrate pollution, the treated water streams by ERN can be used in agriculture irrigation decreasing the need of $NH_3$ production from the energy intensive Haber-Bosch process [16]. The selectivity and kinetics of the ERN process are strongly influenced by the choice of electrocatalytic materials. Previous works have focused on the study of charge transfer processes on platinoid metals (*i.e.*, Pt and Pd) [21]. Despite of their stability and excellent catalytic performance, the use of platinum group elements may prevent the commercialization of electrochemical decentralized treatment units because of their high cost, limited availability that identifies them as endangered elements, and the

68 adverse environmental impacts related to extraction and purification of these scarce metals [18]. Thus,
69 replacement of platinoid metals by earth-abundant, low cost and efficient ERN electrocatalysts is of great
70 interest and must be explored [22].

71 Non-precious transition metal electrocatalysts have been used as replacements for expensive
72 platinum-based electrodes. For instance, earth-abundant materials have shown to catalyze water splitting
73 reactions at different pH conditions [23,24] and Fe-containing electrodes have been reported as efficient
74 oxygen reduction catalysts in alkaline media [25]. Therefore, similar electrocatalytic strategies can be
75 used in ERN processes. Iron catalysts with mixed oxidation states (*i.e.,* $Fe^0$, $Fe^{2+}$, and $Fe^{3+}$) have shown
76 to reduce nitrate to nitrite, ammonia, and nitrogen gas. For example, $Fe(OH)_2$ has been reported to reduce
77 nitrate to ammonia under alkaline conditions. Also, soils and sediments containing Fe(II)-Fe(III)
78 hydroxides, or, greenish rust, have been reported to reduce nitrite to nitrous oxide and ammonia [26]. At
79 lower pH values, nano-sized zero-valent iron (nZVI) enhances the chemical conversion of nitrate to 95-
80 100% [27]. These studies demonstrate that Fe-based electrocatalysts can be used as alternative materials
81 to platinum group elements for ammonia electrogeneration from ERN.

82 ERN is a heterogeneous process that occurs at the surface of the electrode. Thus, modifications and
83 changes at the electrode material, structure or its interface may affect the catalytic performance and
84 selectivity. The aim of this work is to evaluate the competitiveness of magnetite-based electrodes as
85 alternatives to commonly used Pt catalysts for water denitrification and ammonia electrogeneration. In
86 that regard, understanding the effect of the surface functionalization of nano-enabled $Fe_3O_4$ electrodes,
87 such as amine-functionalized $Fe_3O_4$ (3-amino propyl triethoxy silane, APTES, pKa = 10.8), and
88 carboxylic acid-functionalized $Fe_3O_4$ (polyacrylic acid, PAA, pKa = 4.5), on the nitrate reduction
89 mechanism, product selectivity (*i.e.*, $N_2$ vs $NH_3$) and engineering figures of merit become important.
90 Evaluating the influence of surface acidity/basicity on the initial adsorption step of nitrate onto the
91 electrode surface, it is still barely explored in the literature. Additionally, the use of cost-effective

electrodes that rely on earth-abundant materials hold the promise to become a paradigm shift to enable competitive implementation of electrochemically driven technologies.

## 2. Experimental

### *2.1. Chemicals*

Iron (III) chloride of analytical grade was used as the metal precursor for the synthesis of magnetite, and it was purchased from Sigma-Aldrich. Amino termination was obtained through functionalization with 3-aminopropyl triethoxy silane (APTES) provided by Sigma-Aldrich. Poly acrylic acid, ammonium acetate, and ammonium hydroxide (28-30%) were obtained from Fischer Scientific. Ethanol (99.5%) and other organic solvents were obtained from Acros Organics. Analytical-grade sodium sulfate (99 %, Sigma-Aldrich) was used as the supporting electrolyte. Reagent grade sodium nitrate, sodium nitrite, and ammonia sulfate (> 99 %) were supplied by Sigma-Aldrich. Solutions were prepared with nano-pure water obtained from a Millipore Milli-Q system with resistivity >18.2 MΩ cm at 25 ºC.

### *2.2. Synthesis of functionalized magnetite nanoparticles*

Magnetite particles were prepared following a hydrothermal synthesis method [28]. In a round bottom flask, 0.68 g of $FeCl_3 \cdot 6H_2O$ (2.5 mmol) were dissolved in 60 mL of ethylene glycol. Then, 3.8 g of $NH_4Ac$ (50 mmol) was added under continuous magnetic stirring until a clear solution was formed. The resulting mixture was transferred to a 100 mL Teflon-lined autoclave vessel and maintained at 200 ºC for 12 h after which a black precipitate of $Fe_3O_4$ was formed. The solid was recovered by magnetic separation, and sequentially washed with milliQ water (x 3) followed by ethanol (x 3), and finally dried under vacuum at 60 ºC for 6 h. The dried solid was ground into uniform powder using an agate mortar until the material appeared homogenous.

115 Amino terminated magnetite ($Fe_3O_4$-$NH_2$) was obtained by modifying the surface with APTES. The
116 pristine magnetite particles (1.0 g) were dispersed by ultrasonication in 250 mL EtOH/$H_2O$ (1:1 volume)
117 for 30 min under inert $N_2$ atmosphere. Thereafter, 2.5 mL of APTES were added to the mixture while it
118 was vigorously stirred under a nitrogen atmosphere at 40 °C for 4 hours. The functionalized material was
119 recovered using a magnet and washed with milliQ water (x 3) followed by ethanol washing (x 3). The
120 product was dried at room temperature under vacuum for 24 h.
121 Carboxylic acid terminated magnetite ($Fe_3O_4$-COOH) was obtained by modifying the surface with
122 polyacrylic acid. Briefly, the pristine magnetite particles (1.0 g) were dispersed by ultrasonication in 300
123 mL of milliQ water. Then, 100 mL of a 15 wt.% polyacrylic acid solution was added dropwise to the
124 suspension. The mixture was kept under stirring at 75 ºC for 4 h, then the solid was recovered by magnetic
125 separation and washed with milliQ water (x 3) followed by ethanol washing (x 3). The product was dried
126 under vacuum at room temperature for 24 h.
127
128 *2.3. Electrode preparation and electrochemical set-up*
129 Magnetite electrodes were prepared by drop-casting the sample ink onto carbon paper (GDL EC-20-
130 10 from FuelCell Store) for both electrolysis and cyclic voltammetry experiments. In 3 mL scintillation
131 vial, 5 mg of magnetite nanoparticles and 2.5 mg of carbon black (MSE supplies LLC) were dispersed
132 in a mixture of 1.0 mL of isopropanol and 4.5 µL of Nafion® to form the ink. The suspension was
133 sonicated for 15 min to obtain a homogenous dispersion. The ink was loaded into a micropipette and was
134 carefully evenly drop casted onto a 1.5 x 2.5 cm area of carbon paper substrate. After 500 µL were
135 carefully drop-casted onto the carbon paper, it was left to dry on a hot plate at 50 ºC for 1 h. Blank
136 electrodes were prepared following the same procedure without the addition of magnetite nanoparticles
137 to the ink.

The electrochemical nitrate reduction was performed in a 150 mL open undivided batch glass reactor using one anode (Ti/$IrO_2$, DeNora) and one cathode (magnetite electrodes previously synthesized) connected to a TENMA 72-2720 power supply. The electrodes were flat with a geometric area exposed of 3 $cm^2$ (area delimited with Teflon tape) and an intergap distance of 1 cm. Under open air conditions, a constant current intensity of 0.12 A (40 mA $cm^{-2}$, a common value used for ERN) was provided to the system to treat 100 mL of a solution containing 100 mg $NO_3^-$-N $L^{-1}$ [29–31] in 50 mM of $Na_2SO_4$ (pH = 5.81±0.06 and conductivity = 9.50±0.28 mS $cm^{-1}$) at 25 °C during 360 min. The solution was continuously mixed using magnetic stirring at 700 rpm to reduce mass transport limitations between the bulk and the electrode surfaces.

To verify the possible re-oxidation events within the undivided electrochemical cell, individual blank experiments with nitrite (100 mg $NO_2^-$-N $L^{-1}$) and ammonia (100 mg $NH_3$-N $L^{-1}$) in 50 mM of $Na_2SO_4$ were performed. According to Fig. SM-1, nitrite can be partially re-oxidized on the surface of the anode because some nitrate was detected. However, no ammonia oxidation nor volatilization were noticed.

*2.4. Analytical techniques*

The crystalline structure of the synthesized materials was analyzed by X-ray powder diffraction using an *p*-XRD Empyrean 2 PANanalytical diffractometer with a Cu Kα (λ =1.5418 Å) radiation source equipped with a PIXcel [3D] detector with a diffractogram scanning window of 20 - 80°. Fourier-transform infrared spectroscopy (FTIR) was conducted with an Agilent Cary 630 FT-IR spectrometer operated in transmittance mode between 500 $cm^{-1}$ to 4000 $cm^{-1}$. Scanning electron microscopy (SEM) images were recorded using a XL30 ESEM-FEG at 10 kV.

Contact angle measurements were carried out with 4.0 μL of a solution containing 10 mM $NaNO_3$ in 0.1 M $Na_2SO_4$ using Attention – Theta Biolin Scientific equipment, during 10 s to evaluate the surface

161 of carbon paper, $Fe_3O_4$, $Fe_3O_4$-$NH_2$ and $Fe_3O_4$-COOH electrode materials. Tests were performed in
162 quadruplicates.

163 All prepared electrodes were evaluated by cyclic voltammetry (CV) in a three-electrode conventional
164 electrochemical cell and used as working electrodes. Graphite rod was used as the counter electrode, and
165 Ag/AgCl (3.5 M) was used as the reference electrode. Solutions were de-aereated by bubbling $N_2$ gas
166 during 20 min and keeping a $N_2$ atmosphere during electroanalysis. Experiments were operated with an
167 Autolab M204 potentiostat (Metrohm). CVs were measured in 0.1 M $Na_2SO_4$ solution in presence and
168 absence of 10 mM $NaNO_3$ at 50 mV $s^{-1}$.

169 During the electrochemical reduction of nitrate, the pH and conductivity parameters were monitored
170 using Hanna Instruments HI 322 and VWR Scientific Products - EC Model 2052 m, respectively.
171 Samples were withdrawn over time, and the concentration of N-species was analyzed by TNT 835, 839
172 and 830 HACH kits for $NO_3^-$-N, $NO_2^-$-N, and $NH_3$-N, respectively, using HACH DR6000 UV–vis
173 equipment.

174 Nitrate conversion was calculated using Eq. (1).

$$Nitrate\ conversion\ (\%) = \frac{C_{nitrate,i} - C_{nitrate,t}}{C_{nitrate,i}} \times 100 \quad (1)$$

175 where $C_{nitrate,i}$ corresponds to the nitrate concentration at time zero, and $C_{nitrate,t}$ to the nitrate
176 concentration at time ($t$), both in mg $NO_3^-$-N $L^{-1}$.

177 During ERN, N-volatile species, such as $N_2$, NO, $NO_2$ or $N_2O$, may be produced. In this work, it was
178 assumed that the N-gas species formed were most likely corresponding to $N_2$ and its evolution was
179 determined by mass balance. The risk of ammonia volatilization due to gas evolution at the electrodes
180 was disregarded from the blank experiments shown in Fig. SM1b. The selectivity ($S_X$) towards $N_2$ and
181 $NH_3$ was calculated using Eq. (2).

$$S_X(\%) = \frac{C_X}{C_{nitrate,i} - C_{nitrate,t}} \times 100 \quad (2)$$

where $C_X$ represents the concentration (mg N $L^{-1}$) of a species $X$ produced at time $t$. Nitrate reduction was evaluated in terms of Faradaic efficiency (*FE*, Eq. (3)), which determines the number of electrons consumed in an electrochemical reaction relative to the expected theoretical conversion ruled by Faraday's law.

$$FE(\%) = \frac{n\,F\,N_i}{3600\,I\,t} \times 100 \quad (3)$$

where $n$ is the number of electrons required per mol of product (mol), $F$ is the Faraday constant (96 487 C $mol^{-1}$), $N_i$ is the amount (mol) of product generated during the electrolysis, $I$ is the applied electric current (A), $t$ is the electrolysis time (h), and 3600 is a unit conversion factor (3600 s $h^{-1}$).

Electrical energy per order (EE/O), was used as an engineering figure of merit to benchmark the electric energy required to reduce $NO_3^-$-N concentration by one order of magnitude in a unit volume calculated from Eq. (4) for batch operation mode.

$$EE/O(kWh\,m^{-3}order^{-1}) = \frac{E_{cell}\,I\,t}{V_s\,log\,log\,(C_0/C_t)} \quad (4)$$

where $E_{cell}$ is the average of the cell potential (V), $I$ is current intensity (A), $t$ is time (h), $V_s$ is solution volume (L), and $C_0$ and $C_t$ are the initial and final concentration after one order of magnitude reduction. Considering the relationship $\log(C_0/C_t) = 0.4343\,t\,k_1$, where $k_1$ represents first-order kinetics constant ($s^-$

198 [1]), the *EE/O* expression can be simplified assuming according to Eq. (5) where $6.39\times10^{-4}$ is a conversion
199 factor:

$$EE/O(kWh\,m^{-3}order^{-1}) = \frac{6.39 \times 10^{-4}\, E_{cell}\, I}{V_s k_1} \quad (5)$$

200 Experiments were run in duplicate, and the samples withdrawn were analyzed in duplicate to test the
201 precision of the measurement. Deviations between runs were always lower than 5% for all
202 determinations.
203
204 Brief note: Electroanalysis is used to qualitatively study the fundaments of a reaction/characterization of
205 an electrode material; while the electrolysis is considered a real application of these systems to
206 treat/convert pollutants. Hence, the concentrations used in both approaches were specific for the analysis
207 that was being performed within the parameters found in literature.
208
209 **3. Results and discussion**
210 *3.1. Physical characterization of the magnetite particles*
211 The synthesized magnetite nanoparticles were characterized through *p*-XRD in order to assess their
212 crystallinity and through FTIR in order to prove the surface functionalization. The size and morphology
213 of the nanoparticles were determined through SEM. Fig. 1 shows the powder X-ray diffraction (*p*-XRD)
214 pattern of the pristine and functionalized $Fe_3O_4$ samples. The *p*-XRD patterns were obtained in a 2θ range
215 from 20 to 80 degrees. The diffraction pattern for $Fe_3O_4$ nanoparticles was indexed according to JCPDS
216 card no. 19-629. The crystallographic planes (220), (311), (400), (422), (511) and (440) were observed
217 at 2θ = 30.4, 35.8, 37.4, 43.4, 53.7, 57.2 and 62.8°, respectively. The -$NH_2$ and -COOH functionalized

218 $Fe_3O_4$ nanoparticles show the same diffraction patterns which are consistent with crystalline magnetite
219 structures.

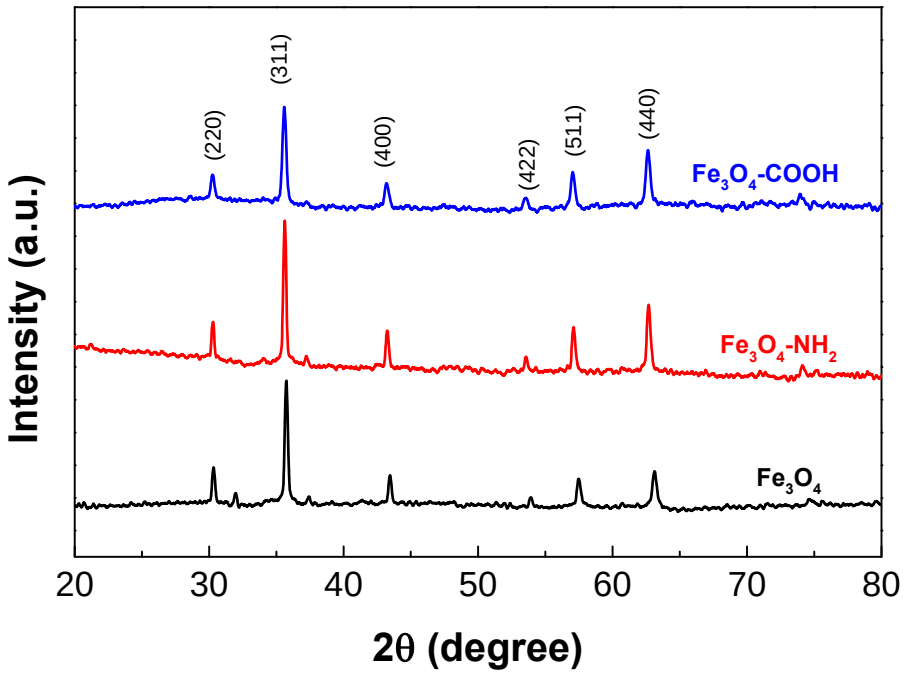


220

221 **Fig. 1 –** *p*-XRD pattern of pristine $Fe_3O_4$ structure (bottom); $NH_2$-functionalized $Fe_3O_4$(middle); and
222 COOH-functionalized $Fe_3O_4$ (top).

223

224 The crystallite size of the nanoparticles was calculated using the Scherrer equation. The full width at
225 half maximum (FWHM) of each diffraction pattern was calculated from the (311) peak for the three
226 samples. The estimated crystallite sizes are: 5.7, 4.5, and 6.6 nm for bare $Fe_3O_4$, $Fe_3O_4$-$NH_2$ and $Fe_3O_4$-
227 COOH, respectively. The average crystallite size for the three $Fe_3O_4$ samples is within the same order of
228 magnitude since the same synthetic procedure was followed prior to surface functionalization.

229 The FTIR spectra of the three $Fe_3O_4$ samples are shown in Fig. 2. The three spectra show a sharp peak
230 corresponding to the Fe-O stretch at 550 $cm^{-1}$ which corroborates the iron oxide nature of all the
231 nanomaterials considered. The FTIR spectrum of bare $Fe_3O_4$ nanoparticles do not show any additional

232 significant peak. The second spectrum corresponding to $Fe_3O_4$ functionalized with APTES ($Fe_3O_4$-$NH_2$)
233 show the characteristic peaks corresponding to the Si-O stretching at 955 $cm^{-1}$ and SiO-H stretching at
234 1070 $cm^{-1}$, which allow inferring the successful surface modification and coordination of APTES to the
235 $Fe_3O_4$ surface. This conclusion is further supported by the two peaks corresponding to N-H stretching
236 observed at 1420 and 2980 $cm^{-1}$. The peak at 2890 $cm^{-1}$ corresponds to a HC-H vibration associated to
237 the alkyl chain. Finally, the spectrum corresponding to the $Fe_3O_4$ functionalized with poly-acrylic acid
238 ($Fe_3O_4$-COOH) shows a peak at 1632-1930 $cm^{-1}$ associated to the C=O bond of the carboxyl group,
239 demonstrating the successful surface functionalization of the nanoparticles. The broad signal centered at
240 3200 $cm^{-1}$ is assigned to the O-H bond stretch from the hydroxyl groups.

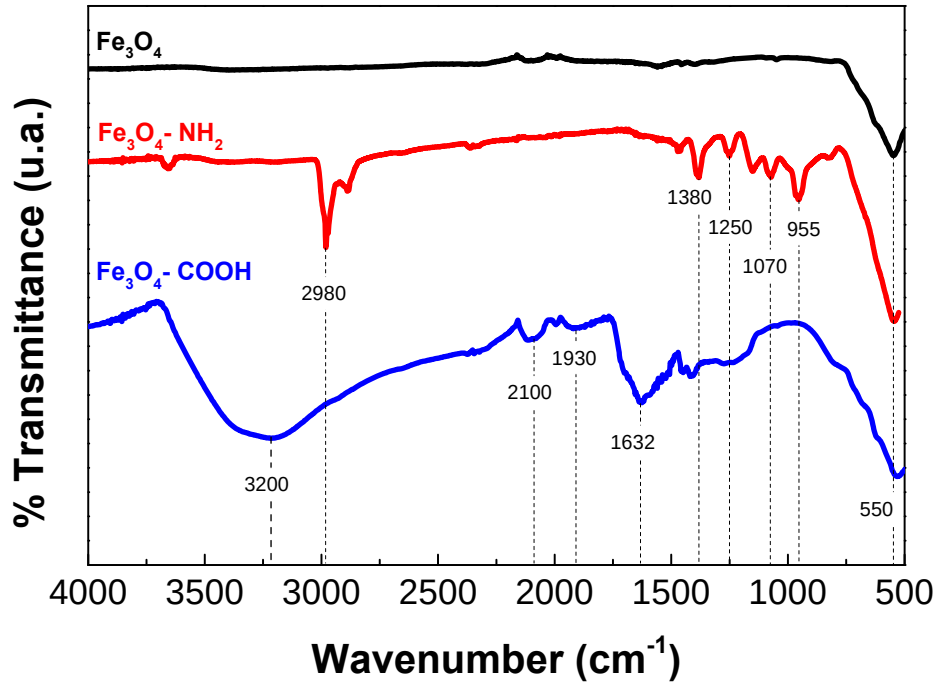


241

242 **Fig. 2 –** FTIR overlay spectra of pristine $Fe_3O_4$ (top), $NH_2$-functionalized $Fe_3O_4$ (middle) and COOH-
243 functionalized $Fe_3O_4$ (bottom).

244

245 Scanning electron microscopy images were obtained to observe the morphology and the size of the as
246 prepared $Fe_3O_4$ nanoparticles and the bare carbon paper substrate. Fig. 3 depicts the two different
247 magnifications that were used to study each material. The surface morphology of bare carbon paper in
248 Fig. 3a shows folds and creases that become clearer at higher magnification in Fig. 3b. Bare $Fe_3O_4$
249 nanoparticles loaded onto the carbon paper substrate have a spherical shape and a size distribution of 250
250 nm and show some aggregation according to Figs. 3c and 3d. Spherical $NH_2$-functionalized $Fe_3O_4$ loaded
251 onto the carbon paper substrate have an average size of 350 nm in diameter and are shown in Fig. 3e and
252 f. These nanoparticles are less aggregated compared to the bare $Fe_3O_4$ due to the amine functionalization.
253 The micrographs corresponding to the $Fe_3O_4$-COOH electrodes (Fig. 3g and 3h) exhibit similar spherical
254 morphology with a diameter of ≈ 500 nm. These COOH-functionalized $Fe_3O_4$ particles are less
255 aggregated when compared to the bare and to the $NH_2$-functionalized nanoparticles. There is a size
256 increase in the diameter of the nanoparticle after functionalization. This is due to the PAA and APTES
257 molecules surrounding the spheres.
258

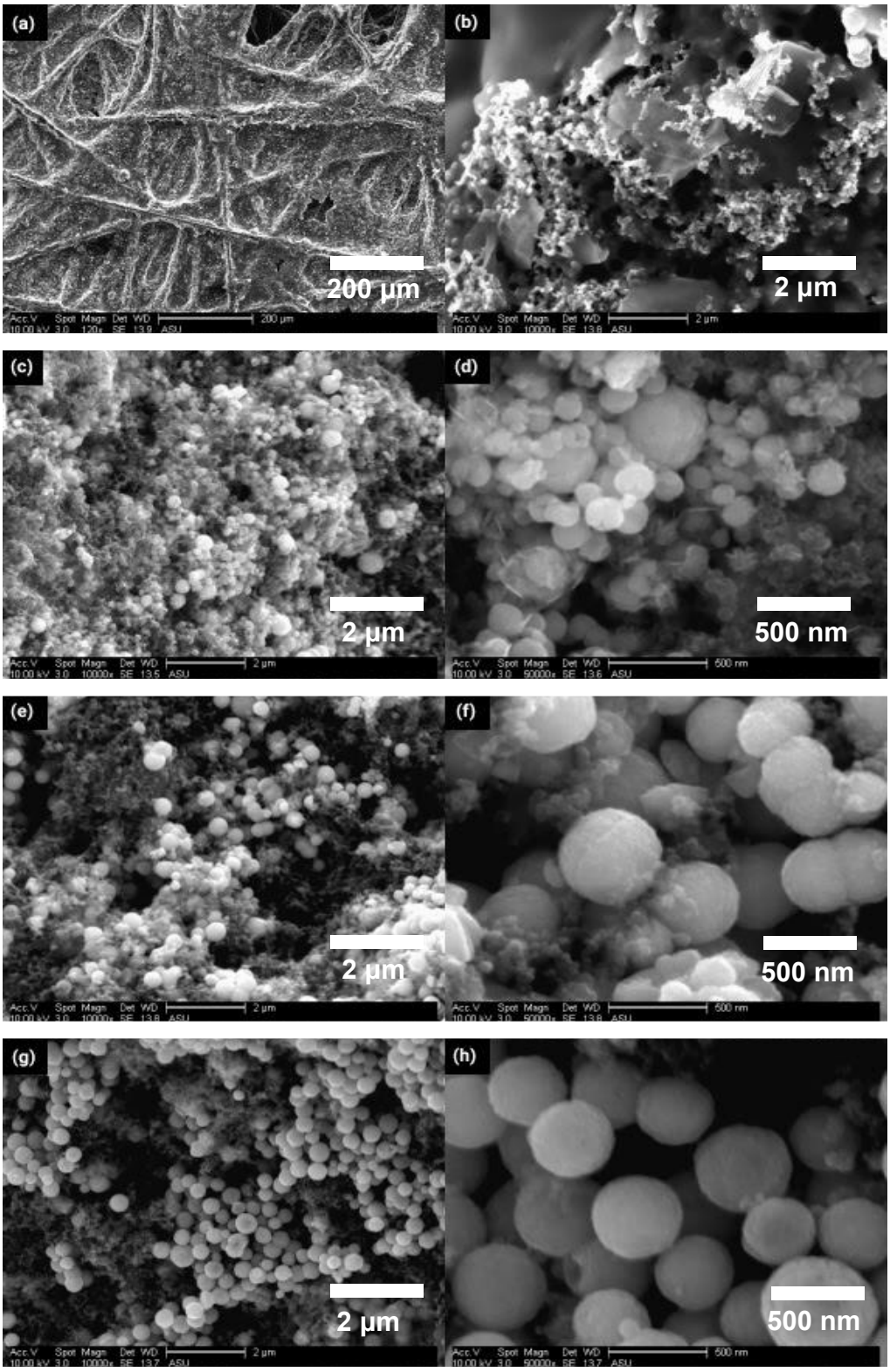


259

**Fig. 3 –** SEM images corresponding to (a,b) carbon paper, (c, d) carbon paper + $Fe_3O_4$, (e, f) carbon paper + $Fe_3O_4$-$NH_2$ and (g, h) carbon paper + $Fe_3O_4$-COOH, at 120X (a), 10,000X of magnitude (b, c, e and g) and at 50,000X of magnitude (b, d, f and h).

Hydrophobic interactions of the electrode surface between the solution and the surface of the catalyst/electrode can affect the electrochemical reduction process of nitrate. Fig. 4 shows the contact angle of the model solution which is in an average of 133° ± 5°, 141° ± 4°, 121° ± 8° and 124° ± 3° for carbon paper, $Fe_3O_4$, $Fe_3O_4$-$NH_2$, $Fe_3O_4$-COOH, respectively, showing that materials are mainly hydrophobic. The functionalized $Fe_3O_4$ electrodes show a decrease in the contact angles (and hydrophobicity) compared to the bare $Fe_3O_4$ electrodes which likely enhances the interaction between their surface and the aqueous solutions. solvent.

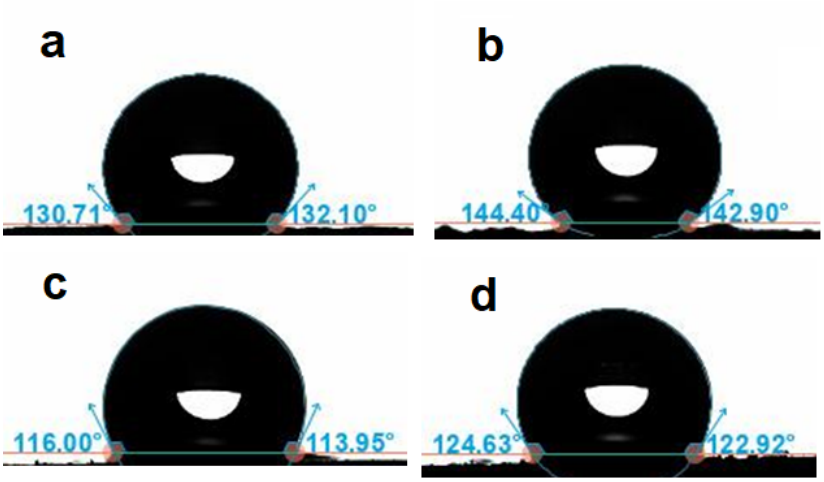


**Fig. 4 –** Contact angle images for droplets of 10 mM $NaNO_3$ in 0.1 M $Na_2SO_4$ on: (a) carbon paper, (b) carbon paper + $Fe_3O_4$, (c) carbon paper + $Fe_3O_4$-$NH_2$ and (d) carbon paper + $Fe_3O_4$-COOH.

### *3.2. Electrochemical characterization of the nano-enabled electrodes*

The electrochemical behavior of the nano-enabled electrodes was evaluated in 0.1 M $Na_2SO_4$ with and without 10 mM $NaNO_3$ using cyclic voltammetry (CV) (Fig. 5). The solution resistance observed in CV shape corresponds to electrode-electrolyte resistance corresponding with the contact angle results, a higher resistance for $Fe_3O_4$ and lower resistance for $Fe_3O_4$-$NH_2$.

For the three electrodes, an oxidation peak (-0.25 V) and reduction peak (-1.2 V) are associated to the oxidation and reduction of iron species contained in $Fe_3O_4$ as previously reported in literature [32–34]. In absence of nitrate, the reduction current density increases starting from -1.25 V due to hydrogen evolution reaction (HER). By comparing the current density displayed in presence and absence of nitrate, it can be concluded that the larger current density displayed in the presence of nitrate in all 3 cases might be attributed to two coexisting processes, nitrate reduction and HER.

The functionalization of $Fe_3O_4$ nanoparticles with APTES presents a similar electrochemical behavior than $Fe_3O_4$ nanoparticles. Despite the contact angle indicates more wettability and better contact of water molecules with electrode surface, it does not provide information related to nitrate transport from/towards the metal oxide surface where the charge transfer takes place. The $Fe_3O_4$ surface linked APTES is a large group that can hinder the transport of $NO_3^-$ due to steric effects or due to the occupation of catalytic sites by the Si-O-Fe bond.

In the case of $Fe_3O_4$-COOH, the electrochemical behavior shows a considerable increment of current density than other electrodes, this could be that carboxyl group promotes the HER [35]. Besides, the results correspond to contact angle result that reported a better interaction of electrolyte and surface than $Fe_3O_4$ nanoparticles.

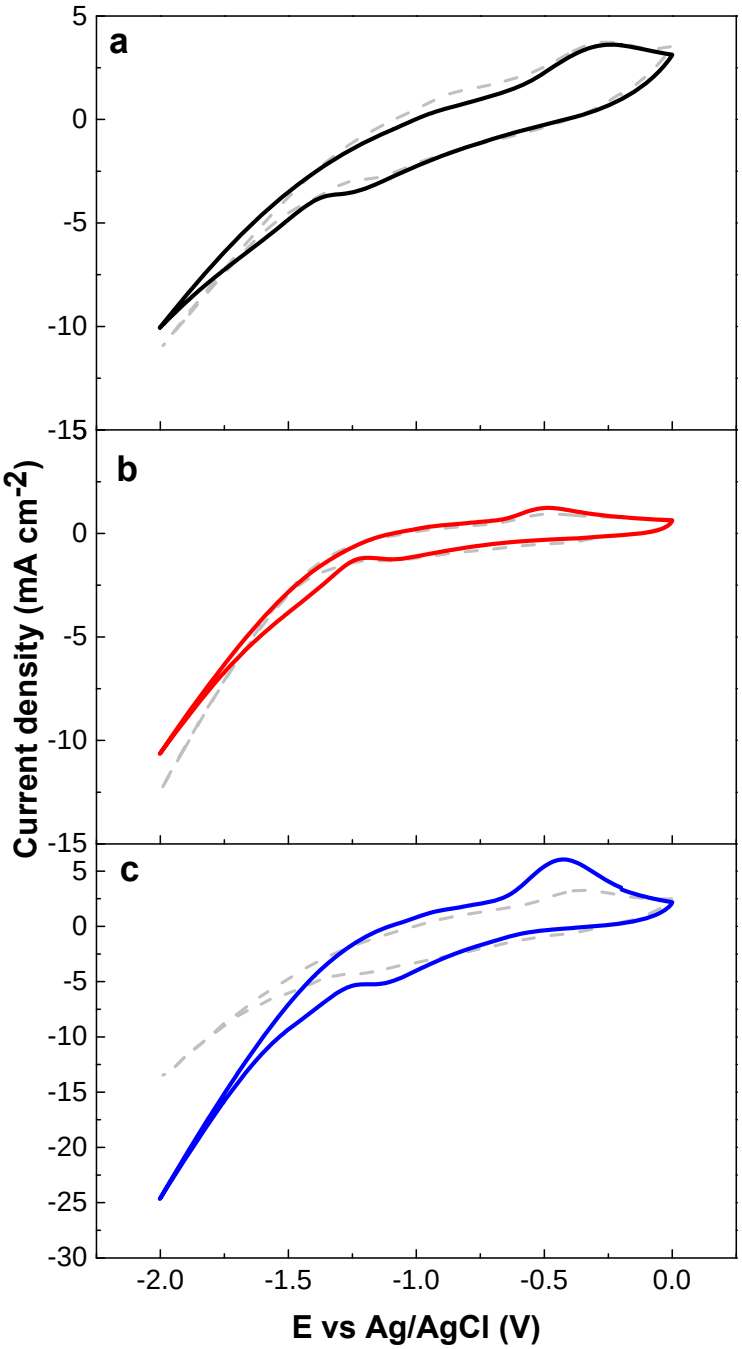


297

298 **Fig. 5 –** Cyclic voltammetry recorded at 50 mV $s^{-1}$ with (a) $Fe_3O_4$, (b) $Fe_3O_4$-$NH_2$, and (c) $Fe_3O_4$-
299 COOH in 0.1 M $Na_2SO_4$ (dash line) and with the presence of 10 mM $NaNO_3$ (solid line). Solutions
300 previously purged with $N_2$ during 20 min.

The electrochemical reduction of nitrate requires the transport of nitrate from the bulk solution to the electrode surface and its subsequent adsorption and it is proposed to occur via inner-sphere electron transfer mechanism. Recent studies suggest the contribution of outer sphere reduction mechanisms that involve the participation of a redox mediator (*i.e.*, $H_{ads}$, $H_2$) [36–38]. The electroanalytical results displayed in Fig.5 show only slight differences in the CV between the three magnetite-based catalysts. This suggests that the functionalized surface of $Fe_3O_4$ electrodes does not control the interaction electrode-electrolyte.

*3.3. Electrocatalytic reduction of nitrate with iron and magnetite electrodes*

The magnetite-based electrodes in this study were benchmarked against a pure Fe plate. Fig. 6a shows the nitrate reduction over time and the evolution of nitrite as well as nitrogen gas and ammonium employing the Fe-plate as cathode. This Fe electrode has a pollutant conversion rate that fits a pseudo first-order reaction with $k_1$ of $5.7\times10^{-5}$ $s^{-1}$ ($R^2$=0.998) and a maximum of 71% of $NO_3^-$-N transformation, after 360 min. These results are consistent to previous studies on Pt and other materials surfaces [22], where the nitrate reduction kinetics on the electrode is controlled by the first charge transfer reaction as limiting step (Eq. 6). The conversion of nitrate to nitrite is based on a three-step electrochemical-chemical-electrochemical (ECE) mechanism as described by Eqs 6 – 8. During the treatment process, the maximum concentration of $NO_2^-$-N was 0.23 mg $L^{-1}$ at 30 min. According to Eq. 9 and Eq.10, the reduction of nitrite generates hydroxide ions which increases the pH of the solution over time from 5.81±0.06 to 11.05±0.04 after 360 min of electrolysis. In this pH range, $N_2$ and $NH_3/NH_4^+$ are the thermodynamically most stable forms of nitrogen according to Frost-Ebsworth diagrams [18,39]. The highest accumulation of nitrite reduction products was obtained after 360 min with concentration values of $N_2$-N = 37.9 mg $L^{-1}$ and $NH_3$-N = 35.9 mg $L^{-1}$. Table 1 summarizes key fitted and calculated parameters

from all the experiments and it shows that the Fe-plate electrode led to a conversion of nitrate of 51% to nitrogen gas ($S_{N_2}$), and of 49% to ammonia ($S_{NH_3}$). Despite the previously reported ability of Fe cathodes to obtain ammonia as the major by-product [40,41], under the specific operating conditions applied in this work, it was observed a balanced selectivity towards ammonia and nitrogen gas. The use of Fe plate yielded a decrease in the nitrate concentration (28.7 mg $L^{-1}$ $NO_3^-$-N) after treatment; however, it did not fall below the maximum contamination level of 10 mg $NO_3^-$-N $L^{-1}$.

$$NO_{3(ad)}^- + e^- \rightarrow NO_{3(ad)}^{2-} \text{ - limiting step} \quad (6)$$

$$NO_{3(ad)}^{2-} + H_2O \rightarrow NO_{2\,(ad)}^{\bullet} + 2OH^- \quad (7)$$

$$NO_{2\,(ad)}^{\bullet} + e^- \rightarrow NO_{2(ad)}^- \quad (8)$$

$$NO_{2\,(ad)}^- + 2H_2O + 3e^- \rightarrow \frac{1}{2}N_{2\,(gas)} + 4OH^- \quad (9)$$

$$NO_{2\,(ad)}^- + 5H_2O + 6e^- \rightarrow NH_3 + 7OH^- \quad (10)$$

As it can be observed in Fig. 6b, using $Fe_3O_4$ nanoparticles deposited on carbon paper, the nitrate conversion was 85% ($k_1$=8.5×$10^{-5}$ $s^{-1}$, $R^2$=0.999). The carbon paper substrate itself has no significant effect on the ERN (Fig. SM2), which highlights the excellent electrocatalytic properties of nano-enabled $Fe_3O_4$ electrodes for nitrate reduction in neutral and slightly alkaline aqueous solution. When using the $Fe_3O_4$, the maximum concentration of $NO_2^-$-N generated occurred after 120 min with 0.63 mg $L^{-1}$, decreasing over time until 0.16 mg $L^{-1}$. This trend can be attributed to a higher generation of ammonia (48.5 mg $L^{-1}$) and nitrogen gas (32.6 mg $L^{-1}$), representing 59% and 40% of their selectivity, respectively. In contrast to Fe plate electrodes, the magnetite-based electrodes have a higher affinity towards ammonia generation. Nitrogen gas is the most desirable product when considering drinking water usage, but ammonia can be an added value product desirable for other applications. For example, an ammonia enriched water may be useful for agriculture irrigation given its fertilizing capabilities. Indeed, attention

has been given recently to the sustainable generation of ammonia by the electrochemical reduction of nitrate due to the opportunity to use that by-product as a fertilizer in crops [42,43].

Table 1 shows that the use of iron oxide nanoparticles has an increase of 1.2 times in the nitrate conversion when compared to the Fe plate electrode. This behavior can be attributed to the increase of active sites available in the presence of $Fe_3O_4$ nanoparticles. Moreover, the use of nano-$Fe_3O_4$ as cathodes for ERN leads to a 45% decrease in the EE/O from 72 kWh $m^{-3}$ $order^{-1}$ for Fe to 41 kWh $m^{-3}$ $order^{-1}$ for $Fe_3O_4$. EE/O values are directly related to the cell potential average ($E_{cell}$) and the kinetics constant for each material (Table 1). If waters with lower conductivity values were used, EE/O would have increased, since conductivity is inversely proportional to $E_{cell}$.

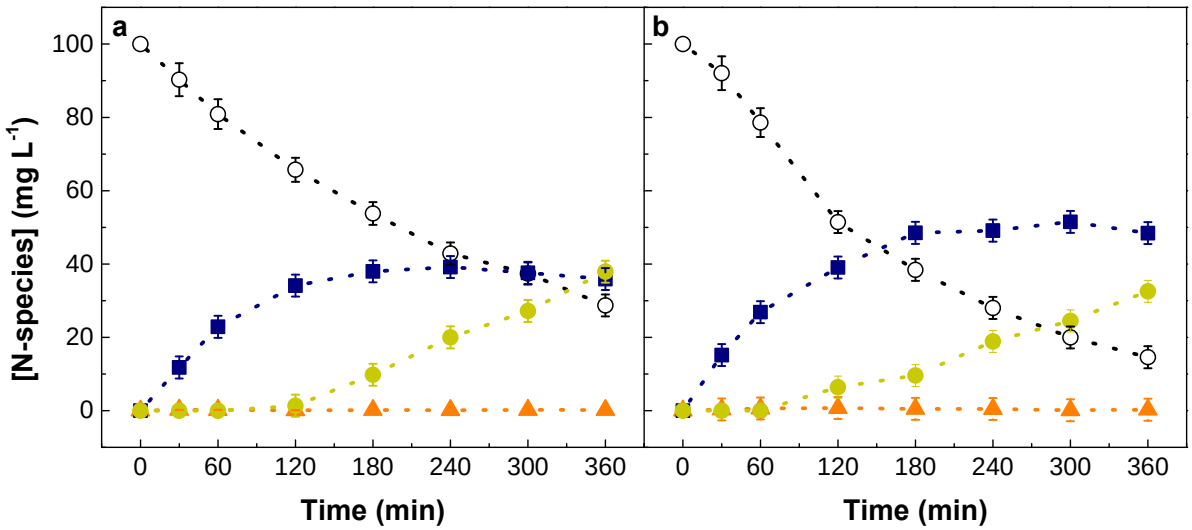


**Fig. 6** - Evolution of the nitrogenated species ((◯) $NO_3^-$-N, (▲) $NO_2^-$-N, (■) $NH_3$-N, and (●) $N_2$-N) over time for the electroreduction of 100 mg $L^{-1}$ $NO_3^-$-N in 50 mM $Na_2SO_4$ at 40 mA $cm^{-2}$ using a) Fe-plate or b) $Fe_3O_4$ as cathodes.

357 *3.4. Influence of magnetite functionalization on the reaction mechanism and product selectivity*

358 To enhance the long-term stability of the nano-$Fe_3O_4$ based electrodes, the $Fe_3O_4$ nanomaterials were
359 surface functionalized with amino- and carboxylic groups. As the $Fe_3O_4$-$NH_2$ electrode has in its
360 composition $NH_2$, a blank experiment with only 50 mM $Na_2SO_4$ was performed as a control to verify if
361 any change occurred on the concentration of the nitrogenous compounds over time. Fig. SM3 shows that
362 null yield of N-species occurs when using $Fe_3O_4$-$NH_2$ electrodes during 360 min of electrolysis, hence
363 not affecting the performance of the process. A gradual reduction of nitrate was observed when
364 conducting electrolysis with $Fe_3O_4$-$NH_2$ cathode as seen in Fig.7a. A maximum abatement of 71% of
365 initial nitrate concentration was reached after 360 min of treatment, with a kinetic constant slightly lower
366 (~1.5x) than the one observed for $Fe_3O_4$ (Table 1). The $NH_2$ functionalization of $Fe_3O_4$ did not improve
367 the performance of nitrate reduction and has similar selectivity values for $NH_3$ (60%) and $N_{gas}$ (38%)
368 products (Table 1). This result is consistent with the information obtained from the cyclic voltammetry
369 (cf. Fig. 5) analysis that depicted a lower electrocatalytic response of $Fe_3O_4$-$NH_2$ electrode in presence
370 of nitrate. The long APTES amine chain in the $Fe_3O_4$-$NH_2$ cathode seems to decrease the interaction
371 between the nitrate and the surface of the electrode. The lower reduction of nitrate may be associated to
372 steric effects and catalytic sites blockage that hinder the transport of nitrate towards the electrode surface,
373 making it difficult both, inner and outer sphere reduction processes. Conversely, a positive effect in
374 activity was observed for the cathode based on $Fe_3O_4$-COOH. The introduction of -COOH functional
375 group (Fig. 7b) led to 90% of nitrate conversion. Meanwhile, the kinetic analysis revealed a higher $k_1$
376 than the decay kinetic constant observed with bare $Fe_3O_4$ nanoparticles (~1.2x higher) (Table 1). In that
377 case, steric effects are not expected to occur given the smaller dimensions of the functional molecule
378 bonded to the bare $Fe_3O_4$ surface. When using the $Fe_3O_4$-COOH electrode, the lowest final nitrogenous
379 concentrations for $NO_3^-$-N (11 mg $L^{-1}$, close to the MCL≈10 mg $L^{-1}$) and $NO_2^-$-N (0.1 mg $L^{-1}$) were

reached, being accompanied by the highest concentrations for $NH_3$-N (50 mg $L^{-1}$) and $N_2$-N (41 mg $L^{-1}$) species. This corresponds to $S_{NH_3}$=55% ($FE_{NH_3}$=11%) and $S_{Ngas}$=45% ($FE_{Ngas}$=5%). It is important to remark that besides leading to the highest decay kinetic constant for nitrate, the $Fe_3O_4$-COOH electrocatalyst reduced nitrate with the lowest EE/O of 37 kWh $m^{-3}$ $order^{-1}$.

Comparing from a global point of view the nitrate conversion (~71 - 90%) and the selectivity towards nitrogen gas (~38 - 45%) and ammonia (~55 - 60%) reached by $Fe_3O_4$ nanoparticles with and without functionalization were only slightly different. These results suggest that the surface driven mechanism expected for an inner sphere process is not the main driver for nitrate reduction when using $Fe_3O_4$-based electrocatalysts in neutral and slight alkaline aqueous solutions. To rule out the contribution of other species that may be electrogenerated during electrolysis under natural conditions, further studies were conducted to disregard impacts of side-reactions such as oxygen reduction reactions (ORR) according to Eqs. (11) – (16) [44].

Acidic electrolyte

$$O_2 + 4H^+ + 4e^- \rightarrow 2H_2O \quad (11)$$

$$O_2 + 2H^+ + 2e^- \rightarrow H_2O_2 \quad (12)$$

$$H_2O_2 + 2H^+ + 2e^- \rightarrow 2H_2O \quad (13)$$

Alkaline electrolyte

$$O_2 + 2H_2O + 4e^- \rightarrow 4OH^- \quad (14)$$

$$O_2 + H_2O + 2e^- \rightarrow HO_2^- + OH^- \quad (15)$$

$$HO_2^- + H_2O + 2e^- \rightarrow 3OH^- \quad (16)$$

The ORR is commonly observed in carbonaceous electrodes [45], and it was detected in aerated cyclic voltammetry (data not shown). ORR is a competitive reaction taking place simultaneously to ERN during electrolysis, which can reduce Faradaic efficiency and yield other electroactive species that can act as

396 redox mediators for nitrate reduction. Therefore, a bulk electrolysis for nitrate removal was conducted in
397 a de-aereated solution bubbling $N_2$ to avoid ORR. No notorious differences in nitrate conversion were
398 observed when compared to the initial experiments without $N_2$ bubbling, so the effect of the ORR during
399 ERN was discarded. Additional blank experiments were conducted to evaluate the impact of coexisting
400 Fenton and Fenton-like reactions through reactions (17) and (18), respectively. These reactions that can
401 be catalyzed by the iron species of the magnetite catalyst yield reactive oxygen species such as hydroxyl
402 radical ($^{\bullet}OH$) and superoxide radical ($O_2^{\bullet-}$) that can engage in different charge transfer reactions
403 [25,26,46]. Nitrate solutions of 100 mg $L^{-1}$ $NO_3^-$-N in 50 mM $Na_2SO_4$ were exposed to 12.5 mM of $H_2O_2$
404 during 360 min without affecting the initial nitrate concentration nor N-species distribution (no reduction
405 observed). Similarly, no variation on the time-course of nitrate concentration was observed when
406 exposing the same solution to a Fenton reaction in presence of 12.5 mM of $H_2O_2$, 0.5 mM of $Fe^{2+}$ and an
407 initial pH of 3.0 for 360 min. From these results, the effect of ORR and other reactive oxygen species
408 that may act as redox mediators were completely excluded as drivers of nitrate reduction.

$$Fe^{2+} + H_2O_2 \longrightarrow Fe^{3+} + {}^{\bullet}OH + OH^- \quad (17)$$

$$Fe^{3+} + H_2O_2 \longrightarrow Fe^{2+} + {}^{\bullet}OOH + H^+ \quad (18)$$

409

410 The fact that nitrate reduction occurs overlapped with hydrogen evolution reaction (Fig. 5) and the
411 small differences observed for different $Fe_3O_4$-functionalized electrocatalysts suggest that hydrogen may
412 play a role in the reduction of nitrate during ERN and the $NO_3^-$ (Eq. 6) adsorption and first electron
413 transfer is not the rate determining reaction step in the mechanism.
414 Thus, ERN occurs through two co-existing pathways on $Fe_3O_4$ nanoparticles: (1) an inner sphere
415 process where adsorption is the most likely limiting step, and (2) an outer sphere process through a
416 hydrogen based redox mediator species electrogenerated at negative potentials on the $Fe_3O_4$ surface.

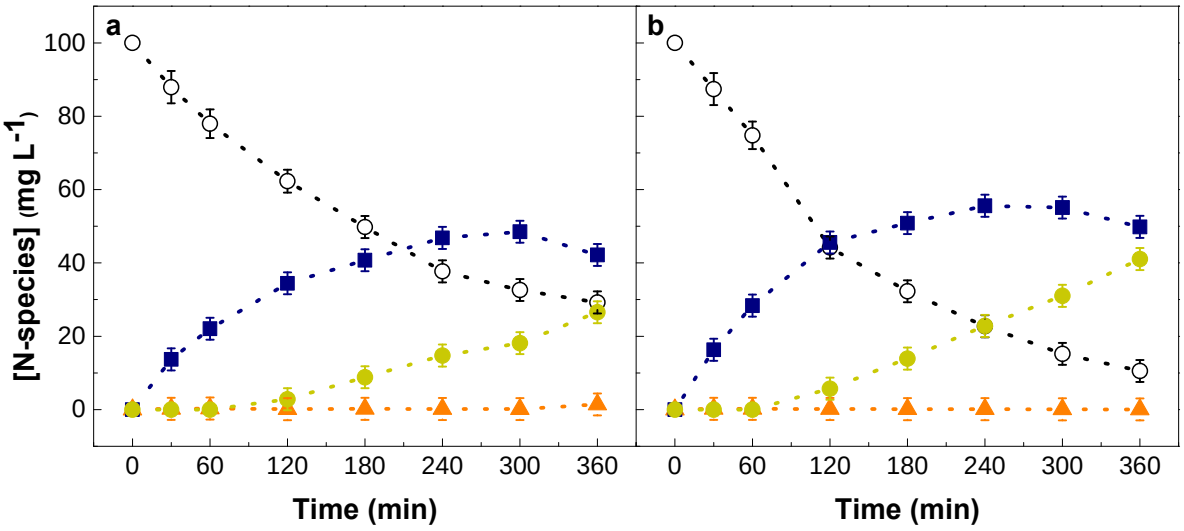


417

418 **Fig. 7** - Evolution of the nitrogenated species ((◯) $NO_3^-$-N, (▲) $NO_2^-$-N, (■) $NH_3$-N, and (●) $N_2$-N)

419 over time for the electroreduction of 100 mg $L^{-1}$ $NO_3^-$-N in 50 mM $Na_2SO_4$ at 40 mA $cm^{-2}$ using a)

420 $Fe_3O_4$-$NH_2$ or b) $Fe_3O_4$-COOH materials as cathodes.

421

422 **Table 1 –** Average of the cell potential and key fitted/calculated parameters from all the experiments for

423 the electroreduction of 100 mg $L^{-1}$ $NO_3^-$-N in 50 mM $Na_2SO_4$ at 40 mA $cm^{-2}$ and 360 min of treatment

424 time.

| Electrode material | $E_{cell}$ (V) | $k_1$ x $10^{-5}$ ($s^{-1}$) | NC (%) | $S_{Ngas}$ (%) | $S_{NH_3}$ (%) | $FE_{Ngas}$ (%) | $FE_{NH_3}$ (%) | EE/O (kWh $m^{-3}$ $order^{-1}$) |
|---|---|---|---|---|---|---|---|---|
| Fe-plate | 5.35 | 5.7 | 71 | 51 | 49 | 5 | 8 | 72 |
| $Fe_3O_4$ | 4.78 | 8.9 | 85 | 40 | 59 | 4 | 10 | 41 |
| $Fe_3O_4$-$NH_2$ | 5.25 | 6.1 | 71 | 38 | 60 | 4 | 9 | 66 |
| $Fe_3O_4$-COOH | 4.91 | 10.3 | 90 | 45 | 55 | 5 | 11 | 37 |

425

426

## 4. Conclusions

In this work, earth abundant $Fe_3O_4$ nanoparticle-based electrodes were synthesized and tested as model mineral iron oxide for the electrochemical reduction of nitrate (ERN) under easy-to-handle experimental conditions. The effect of the functionalization of the $Fe_3O_4$ nanoparticles, with amine and carboxylic acids groups, was studied to identify sustainable electrocatalytic systems that can remove nitrate from drinking waters. Initially, bare $Fe_3O_4$ nanoparticle-based electrodes were benchmarked against a Fe-plate, being demonstrated the superiority of using cathodes with iron nanoparticles because of the increase of active sites. In fact, $Fe_3O_4$ nanoparticle-based electrodes increased ~1.2x nitrate conversion and led to a decrease in the electric energy por order of ~45%. Regarding the functionalization of $Fe_3O_4$ with organic groups, there were slightly differences when applying these materials to the ERN. While $Fe_3O_4$-$NH_2$ did not improve the performance of the reduction process, $Fe_3O_4$-COOH led to the best results in 360 min, with 90% nitrate conversion ($k_1$=10.3×$10^{-5}$ $s^{-1}$, $R^2$=0.999), 55% selectivity towards ammonia, 11% faradaic efficiency for $NH_3$ generation and the lowest electric energy per order with 37 kWh $m^{-3}$ $order^{-1}$. According to the results, the surface functionalization of $Fe_3O_4$ demonstrated that nitrate adsorption and first electron transfer is not the rate determining reaction step in the electrocatalytic reduction of nitrate mechanism on $Fe_3O_4$ nanoparticles in neutral-alkaline pH solution. An outer sphere process occurring through the hydrogen based redox mediator species electrogenerated on the cathode surface seems to be the dominant process in the ERN.

This work reveals that mineral $Fe_3O_4$ particles can be potentially useful as electrode material for nitrate reduction in natural water sources, representing a green water denitrification treatment option and a sustainable method to recover ammonia to be used as enriched water for crop field irrigation.

**Acknowledgments**

This work was supported by the NSF Nanosystems Engineering Research Center for Nanotechnology-Enabled Water Treatment (NEWT) (ERC-1449500), and by the Welch foundation under grant AH-2083-20210327. Dr. Ana S. Fajardo acknowledges the received funding from the European Union's Horizon 2020 research and innovation program under the Marie Sklodowska-Curie grant agreement No 843870. We thank De Nora Tech, LLC for kindly providing the DSA® electrodes used as anode in our electrochemical system. We acknowledge the use of facilities within the Eyring Materials Center at Arizona State University supported in part by NNCI-ECCS-1542160.

458 **References**


459 [1] D. Han, M.J. Currell, G. Cao, Deep challenges for China's war on water pollution, Environ. Pollut.
460 218 (2016) 1222–1233. https://doi.org/10.1016/j.envpol.2016.08.078.

461 [2] WHO, Nitrate and nitrite in drinking-water, 2016.
462 https://www.who.int/water_sanitation_health/dwq/chemicals/nitrate-nitrite-background-
463 jan17.pdf?ua=1.

464 [3] EPA, National primary drinking water regulations, 2017. https://www.epa.gov/ground-water-and-
465 drinking-water/national-primary-drinking-water-regulations.

466 [4] Y. Zhai, Y. Lei, J. Wu, Y. Teng, J. Wang, X. Zhao, X. Pan, Does the groundwater nitrate pollution
467 in China pose a risk to human health? A critical review of published data, Environ. Sci. Pollut.
468 Res. 24 (2017) 3640–3653. https://doi.org/10.1007/s11356-016-8088-9.

469 [5] M. Allaire, H. Wu, U. Lall, National trends in drinking water quality violations, Proc. Natl. Acad.
470 Sci. U. S. A. 115 (2018) 2078–2083. https://doi.org/10.1073/pnas.1719805115.

471 [6] B.M. Afzal, Drinking water and women's health, J. Midwifery Women's Heal. 51 (2006) 12–18.
472 https://doi.org/10.1016/j.jmwh.2005.08.014.

473 [7] US EPA, National Primary Drinking Water Regulations, 2017. https://www.epa.gov/ground-
474 water-and-drinking-water/national-primary-drinking-water-regulations#Inorganic.

475 [8] D.C. Gooddy, D.J. Lapworth, S.A. Bennett, T.H.E. Heaton, P.J. Williams, B.W.J. Surridge, A
476 multi-stable isotope framework to understand eutrophication in aquatic ecosystems, Water Res.
477 88 (2016) 623–633. https://doi.org/10.1016/j.watres.2015.10.046.

478 [9] Z. Wu, Y. Liu, Z. Liang, S. Wu, H. Guo, Internal cycling, not external loading, decides the nutrient
479 limitation in eutrophic lake: A dynamic model with temporal Bayesian hierarchical inference,
480 Water Res. 116 (2017) 231–240. https://doi.org/10.1016/j.watres.2017.03.039.

481 [10] M.J. Pennino, J.E. Compton, S.G. Leibowitz, Trends in Drinking Water Nitrate Violations Across

the United States, Environ. Sci. Technol. 51 (2017) 13450–13460. https://doi.org/10.1021/acs.est.7b04269.

[11] EPA, Estimated nitrate concentrations in groundwater used for drinking, 2017. https://www.epa.gov/nutrient-policy-data/estimated-nitrate-concentrations-groundwater-used-drinking.

[12] L. Liu, E. Lopez, L. Dueñas-osorio, L. Stadler, Y. Xie, P.J.J. Alvarez, Q. Li, Distributed Direct Potable Water Reuse, Nat. Sustain. 3 (2020) 548–555.

[13] M. Safari, A. Rezaee, B. Ayati, A. Jonidi-Jafari, Bio-electrochemical reduction of nitrate utilizing MWCNT supported on carbon base electrodes: A comparison study, J. Taiwan Inst. Chem. Eng. 45 (2014) 2212–2216. https://doi.org/10.1016/j.jtice.2014.05.006.

[14] T.M. Mubita, J.E. Dykstra, P.M. Biesheuvel, A. van der Wal, S. Porada, Selective adsorption of nitrate over chloride in microporous carbons, Water Res. 164 (2019) 114885. https://doi.org/10.1016/j.watres.2019.114885.

[15] H.S. Shin, Sensitive determination of bromate in ozonated and chlorinated water, and sea water by gas chromatography-mass spectrometry after derivatization, J. Chromatogr. A. 1223 (2012) 136–141. https://doi.org/10.1016/j.chroma.2011.12.059.

[16] S. Hamid, S. Bae, W. Lee, M.T. Amin, A.A. Alazba, Catalytic Nitrate Removal in Continuous Bimetallic Cu-Pd/Nanoscale Zerovalent Iron System, Ind. Eng. Chem. Res. 54 (2015) 6247–6257. https://doi.org/10.1021/acs.iecr.5b01127.

[17] I. Katsounaros, G. Kyriacou, Influence of nitrate concentration on its electrochemical reduction on tin cathode: Identification of reaction intermediates, Electrochim. Acta. 53 (2008) 5477–5484. https://doi.org/10.1016/j.electacta.2008.03.018.

[18] S. Garcia-Segura, M. Lanzarini-Lopes, K. Hristovski, P. Westerhoff, Electrocatalytic reduction of nitrate: Fundamentals to full-scale water treatment applications, Appl. Catal. B Environ. 236

(2018) 546–568. https://doi.org/10.1016/j.apcatb.2018.05.041.

[19] G.F. Chen, Y. Yuan, H. Jiang, S.Y. Ren, L.X. Ding, L. Ma, T. Wu, J. Lu, H. Wang, Electrochemical reduction of nitrate to ammonia via direct eight-electron transfer using a copper–molecular solid catalyst, Nat. Energy. 5 (2020) 605–613. https://doi.org/10.1038/s41560-020-0654-1.

[20] Z.-Y. Wu, M. Karamad, X. Yong, Q. Huang, D.A. Cullen, P. Zhu, C. Xia, Q. Xiao, M. Shakouri, F.-Y. Chen, J.Y. Kim, Y. Xia, K. Heck, Y. Hu, M.S. Wong, Q. Li, I. Gates, S. Siahrostami, H. Wang, Electrochemical ammonia synthesis via nitrate reduction on Fe single atom catalyst, Nat. Commun. 12 (2021) 1–10. https://doi.org/10.1038/s41467-021-23115-x.

[21] G. Tokazhanov, E. Ramazanova, S. Hamid, S. Bae, W. Lee, Advances in the catalytic reduction of nitrate by metallic catalysts for high efficiency and N2 selectivity: A review, Chem. Eng. J. 384 (2020) 123252. https://doi.org/10.1016/j.cej.2019.123252.

[22] A.S. Fajardo, P. Westerhoff, C.M. Sanchez-Sanchez, S. Garcia-Segura, Earth-abundant elements a sustainable solution for electrocatalytic reduction of nitrate, Appl. Catal. B Environ. 281 (2021) 119465. https://doi.org/10.1016/j.apcatb.2020.119465.

[23] F. Dionigi, P. Strasser, NiFe-Based (Oxy)hydroxide Catalysts for Oxygen Evolution Reaction in Non-Acidic Electrolytes, Adv. Energy Mater. 6 (2016). https://doi.org/10.1002/aenm.201600621.

[24] J. Kibsgaard, I. Chorkendorff, Considerations for the scaling-up of water splitting catalysts, Nat. Energy. 4 (2019) 430–433. https://doi.org/10.1038/s41560-019-0407-1.

[25] E. Expósito, C.M. Sánchez-Sánchez, V. Montiel, Mineral Iron Oxides as Iron Source in Electro-Fenton and Photoelectro-Fenton Mineralization Processes, J. Electrochem. Soc. 154 (2007) E116. https://doi.org/10.1149/1.2744134.

[26] B.M. Hunter, J.R. Winkler, H.B. Gray, Iron is the active site in nickel/iron water oxidation electrocatalysts, Molecules. 23 (2018). https://doi.org/10.3390/molecules23040903.

[27] H.C.B. Hansen, C.B. Koch, H. Nancke-Krogh, O.K. Borggaard, J. Sørensen, Abiotic nitrate reduction to ammonium: Key role of green rust, Environ. Sci. Technol. 30 (1996) 2053–2056. https://doi.org/10.1021/es950844w.

[28] D. Yang, J. Hu, S. Fu, Controlled synthesis of Magnetite-silica nanocomposites via a seeded sol-gel approach, J. Phys. Chem. C. 113 (2009) 7646–7651. https://doi.org/10.1021/jp900868d.

[29] M.H. Ward, R.R. Jones, J.D. Brender, T.M. de Kok, P.J. Weyer, B.T. Nolan, C.M. Villanueva, S.G. van Breda, Drinking water nitrate and human health: An updated review, Int. J. Environ. Res. Public Health. 15 (2018) 1–31. https://doi.org/10.3390/ijerph15071557.

[30] M.J. Pennino, S.G. Leibowitz, J.E. Compton, R.A. Hill, R.D. Sabo, Patterns and predictions of drinking water nitrate violations across the conterminous United States, Sci. Total Environ. 722 (2020) 137661. https://doi.org/10.1016/j.scitotenv.2020.137661.

[31] S. Garcia-Segura, A.B. Nienhauser, A.S. Fajardo, R. Bansal, C.L. Coonrod, J.D. Fortner, M. Marcos-Hernández, T. Rogers, D. Villagran, M.S. Wong, P. Westerhoff, Disparities between experimental and environmental conditions: Research steps toward making electrochemical water treatment a reality, Curr. Opin. Electrochem. 22 (2020) 9–16. https://doi.org/10.1016/j.coelec.2020.03.001.

[32] Z.A. Jonoush, A. Rezaee, A. Ghaffarinejad, Electrocatalytic nitrate reduction using Fe0/Fe3O4 nanoparticles immobilized on nickel foam: Selectivity and energy consumption studies, J. Clean. Prod. 242 (2020) 118569. https://doi.org/10.1016/j.jclepro.2019.118569.

[33] D. Huang, Y. Luo, S. Li, M. Wang, Y. Shen, Hybrid of Fe@Fe3O4 core-shell nanoparticle and iron-nitrogen-doped carbon material as an efficient electrocatalyst for oxygen reduction reaction, Electrochim. Acta. 174 (2015) 933–939. https://doi.org/10.1016/j.electacta.2015.06.054.

[34] K. Parvez, S. Yang, Y. Hernandez, A. Winter, A. Turchanin, X. Feng, Nitrogen-Doped Graphene and Its Iron-Based Composite As E ffi cient Electrocatalysts for Oxygen Reduction, (2012) 9541–

554 9550.
555 [35] J.Y. Bai, L.J. Wang, Y.J. Zhang, C.F. Wen, X.L. Wang, H.G. Yang, Carboxyl functionalized
556 graphite carbon nitride for remarkably enhanced photocatalytic hydrogen evolution, Appl. Catal.
557 B Environ. 266 (2020) 118590. https://doi.org/10.1016/j.apcatb.2020.118590.
558 [36] L. Mattarozzi, S. Cattarin, N. Comisso, N. El Habra, P. Guerriero, M. Musiani, L. Vázquez-
559 Gómez, Electrodeposition of compact Ag–Ni films from concentrated chloride baths and their test
560 in the reduction of nitrate in alkali, Electrochim. Acta. 346 (2020).
561 https://doi.org/10.1016/j.electacta.2020.136240.
562 [37] S. Huo, S. Yang, Q. Niu, F. Yang, L. Song, Synthesis of functional Ni2P/CC catalyst and the
563 robust performances in hydrogen evolution reaction and nitrate reduction, Int. J. Hydrogen
564 Energy. 45 (2020) 4015–4025. https://doi.org/10.1016/j.ijhydene.2019.11.210.
565 [38] A. Manzo-Robledo, C. Lévy-Clément, N. Alonso-Vante, The interplay between hydrogen
566 evolution reaction and nitrate reduction on boron-doped diamond in aqueous solution: The effect
567 of alkali cations, Electrochim. Acta. 117 (2014) 420–425.
568 https://doi.org/10.1016/j.electacta.2013.11.151.
569 [39] V.K. Sharma, Oxidation of nitrogen-containing pollutants by novel ferrate(VI) technology: A
570 review, J. Environ. Sci. Heal. - Part A Toxic/Hazardous Subst. Environ. Eng. 45 (2010) 645–667.
571 https://doi.org/10.1080/10934521003648784.
572 [40] M. Li, C. Feng, Z. Zhang, N. Sugiura, Efficient electrochemical reduction of nitrate to nitrogen
573 using Ti/IrO2-Pt anode and different cathodes, Electrochim. Acta. 54 (2009) 4600–4606.
574 https://doi.org/10.1016/j.electacta.2009.03.064.
575 [41] W. Li, C. Xiao, Y. Zhao, Q. Zhao, R. Fan, J. Xue, Electrochemical Reduction of High-
576 Concentrated Nitrate Using Ti/TiO2 Nanotube Array Anode and Fe Cathode in Dual-Chamber
577 Cell, Catal. Letters. 146 (2016) 2585–2595. https://doi.org/10.1007/s10562-016-1894-3.

578 [42] D. Hao, Z. gang Chen, M. Figiela, I. Stepniak, W. Wei, B.J. Ni, Emerging alternative for artificial
579 ammonia synthesis through catalytic nitrate reduction, J. Mater. Sci. Technol. 77 (2021) 163–168.
580 https://doi.org/10.1016/j.jmst.2020.10.056.
581 [43] P.H. van Langevelde, I. Katsounaros, M.T.M. Koper, Electrocatalytic Nitrate Reduction for
582 Sustainable Ammonia Production, Joule. 5 (2021) 290–294.
583 https://doi.org/10.1016/j.joule.2020.12.025.
584 [44] Y. Li, Q. Li, H. Wang, L. Zhang, D.P. Wilkinson, J. Zhang, Recent Progresses in Oxygen
585 Reduction Reaction Electrocatalysts for Electrochemical Energy Applications, Electrochem.
586 Energy Rev. 2 (2019) 518–538. https://doi.org/10.1007/s41918-019-00052-4.
587 [45] R. Ma, G. Lin, Y. Zhou, Q. Liu, T. Zhang, G. Shan, M. Yang, J. Wang, A review of oxygen
588 reduction mechanisms for metal-free carbon-based electrocatalysts, Npj Comput. Mater. 5 (2019).
589 https://doi.org/10.1038/s41524-019-0210-3.
590 [46] A.J. dos Santos, A.S. Fajardo, M.S. Kronka, S. Garcia-Segura, M.R.V. Lanza, Effect of
591 electrochemically-driven technologies on the treatment of endocrine disruptors in synthetic and
592 real urban wastewater, Electrochim. Acta. 376 (2021) 138034.
593 https://doi.org/10.1016/j.electacta.2021.138034.
594
595

# Effect of surface functionalization of $Fe_3O_4$ nano-enabled electrodes on the electrochemical reduction of nitrate

Mariana Marcos-Hernández[a,b], Gabriel Antonio Cerrón-Calle[a,c], Yulu Ge[a,b], , Sergi Garcia-Segura[a,c], Carlos M. Sánchez-Sánchez[d], Ana S. Fajardo[a,c,d,*], Dino Villagrán[a,b,**]

[a]*Nanosystems Engineering Research Center for Nanotechnology-Enabled Water Treatment*

[b]*Department of Chemistry and Biochemistry, The University of Texas at El Paso, El Paso, TX 79968, USA*

[c]*School of Sustainable Engineering and the Built Environment, Arizona State University, Tempe, Arizona 85287-3005, United States*

[d]*Sorbonne Université, CNRS, Laboratoire Interfaces et Systèmes Electrochimiques (LISE), 4 place Jussieu, F-75005, Paris, France*

*Article submitted to be published in Separation and Purification Technology*

**Corresponding author**

***Ana Sofia Fajardo, E-mail: adossan3@asu.edu

****Dino Villagran, E-mail: dino@utep.edu

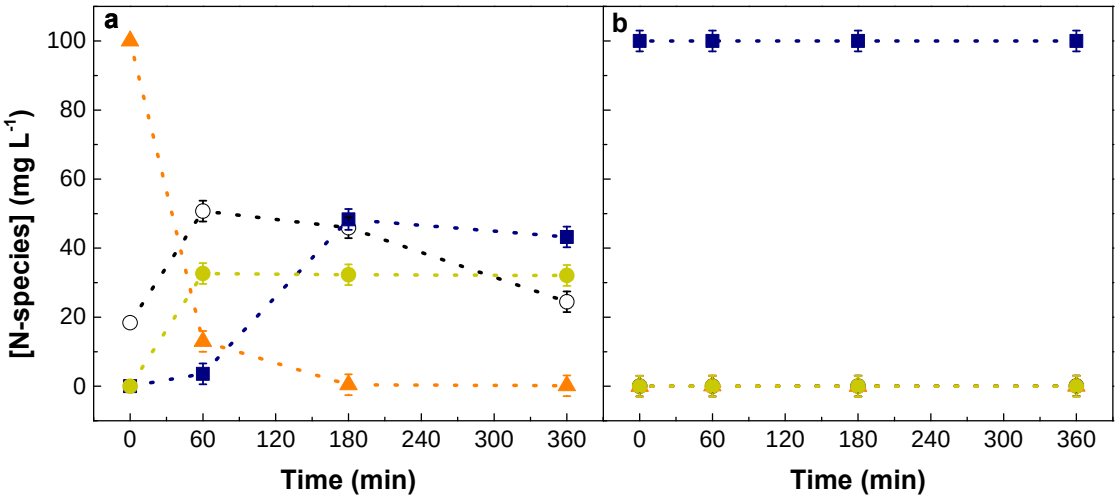


616

617 **Fig. SM1 –** Evolution of the nitrogenated species ((◯) $NO_3^-$-N, (▲) $NO_2^-$-N, (■) $NH_3$-N, and (●) $N_2$-

618 N) over time for the electroreduction of a) 100 mg $NO_2^-$-N $L^{-1}$ and b) 100 mg $NH_3$-N $L^{-1}$ in 50 mM

619 $Na_2SO_4$ at 40 mA $cm^{-2}$ using $Fe_3O_4$-COOH as cathode.

620

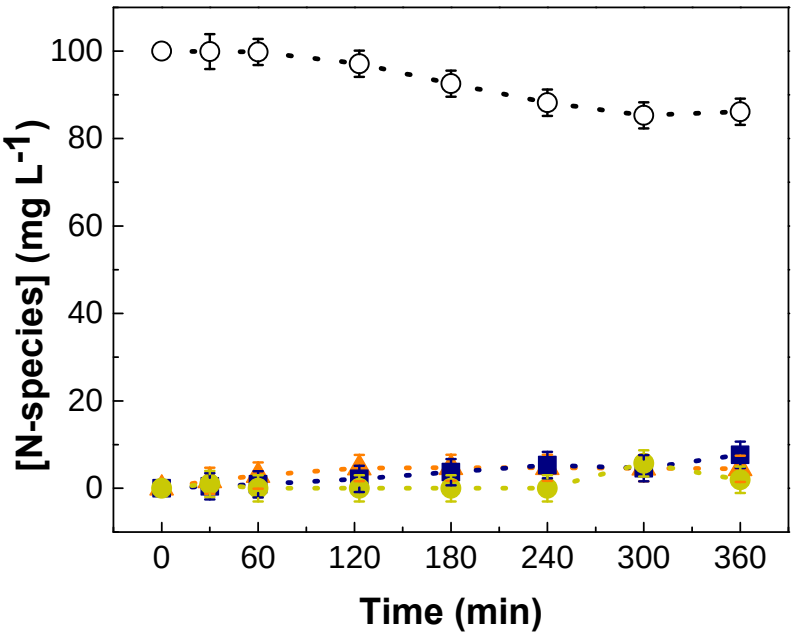


621

622 **Fig. SM2 -** Evolution of the nitrogenated species ((◯) $NO_3^-$-N, (▲) $NO_2^-$-N, (■) $NH_3$-N, and (●) $N_2$-N)

623 over time for the electroreduction of 100 mg $L^{-1}$ $NO_3^-$-N in 50 mM $Na_2SO_4$ at 40 mA $cm^{-2}$ using carbon

624 paper as cathode.

625

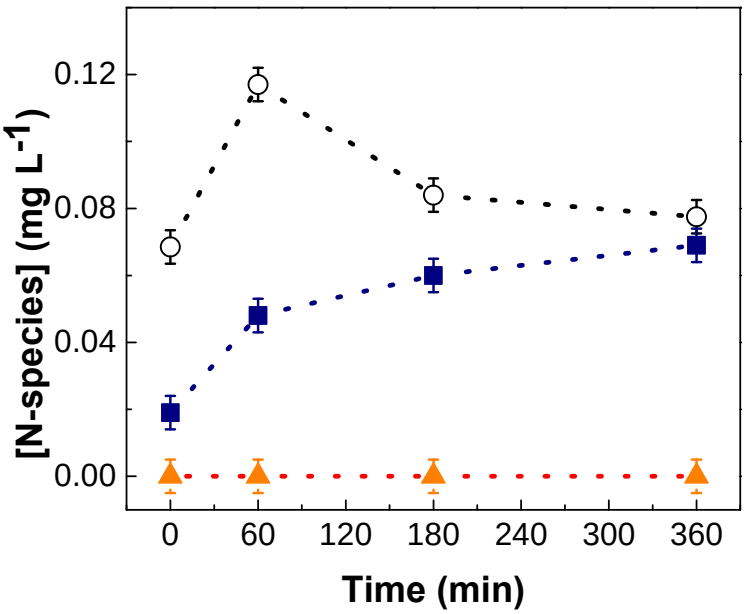


626

627 **Fig. SM3** - Evolution of the nitrogenated species ((◯) $NO_3^-$-N, (▲) $NO_2^-$-N and (■) $NH_3$-N over time

628 for the electrolysis of 50 mM $Na_2SO_4$ at 40 mA $cm^{-2}$ using $Fe_3O_4$-$NH_2$ as cathode.

629

630